Oxidation state and local structure of a high-capacity LiF/Fe(V2O5) conversion cathode for Li-ion batteries

ARTICLE *in* ACTA MATERIALIA · APRIL 2014

Impact Factor: 4.47 · DOI: 10.1016/j.actamat.2014.01.016

9 AUTHORS, INCLUDING:

Ralf Witte
Karlsruhe Institute of Technology
8 PUBLICATIONS **21** CITATIONS

SEE PROFILE

Jörg Rothe
Karlsruhe Institute of Technology
120 PUBLICATIONS **1,220** CITATIONS

SEE PROFILE

Alexander Soldatov
Southern Federal University
221 PUBLICATIONS **1,347** CITATIONS

SEE PROFILE

Maximilian Fichtner
Helmholtz-Institute Ulm
211 PUBLICATIONS **3,215** CITATIONS

SEE PROFILE

Available online at www.sciencedirect.com

ScienceDirect

Acta Materialia 68 (2014) 179–188

Acta MATERIALIA

www.elsevier.com/locate/actamat

Oxidation state and local structure of a high-capacity LiF/Fe(V_2O_5) conversion cathode for Li-ion batteries

A.H. Pohl [a,*], A.A. Guda [b], V.V. Shapovalov [b], R. Witte [a,c], B. Das [a,d], F. Scheiba [e], J. Rothe [f], A.V. Soldatov [b], M. Fichtner [a,d]

[a] Institute of Nanotechnology, Karlsruhe Institute of Technology, PO Box 3640, 76021 Karlsruhe, Germany
[b] Research Center for Nanoscale Structure of Matter, Southern Federal University, 5 Zorge St, 344090 Rostov-on-Don, Russian Federation
[c] Joint Research Laboratory Nanomaterials, Technische Universität Darmstadt, Petersenstr. 32, 64287 Darmstadt, Germany
[d] Helmholtz Institute Ulm, Albert-Einstein Allee 11, 89081 Ulm, Germany
[e] Institute of Applied Materials, Karlsruhe Institute of Technology, PO Box 3640, 76021 Karlsruhe, Germany
[f] Institute for Nuclear Waste Disposal, Karlsruhe Institute of Technology, PO Box 3640, 76021 Karlsruhe, Germany

Received 23 October 2013; received in revised form 16 December 2013; accepted 9 January 2014

Abstract

We prepared LiF/Fe(V_2O_5) nanocomposites with varying (0–20 wt.%) V_2O_5 by high-energy ball milling and found a stable specific capacity of 450 mA h g^{-1} for a period of 20 cycles without a noticeable reduction in capacity for the composite with 15 wt.% V_2O_5. X-ray diffraction was unable to identify new phases present in the nanocomposite. To identify the phases formed during ball milling and cycling, we collected in situ X-ray absorption spectra at the Fe K- and V K-edges. During the first charge, LiF/Fe was converted to ~35% FeF_2, and during the second discharge, the initial $V^{3.9+}$ oxidation state was reduced to $V^{3.5+}$. Using principal component analysis, we decomposed the series of Fe K-edge spectra into three components consisting of Fe, FeF_2 and a new phase, which was identified by comparison with theoretical X-ray absorption near edge structure spectra of model compounds with tetrahedral and octahedral V coordination and ^{57}Fe Mössbauer spectroscopy to be the inverse spinel V[FeV]O_4. From the calculations, we also identified the lithium vanadate $Li_xVO_{2-x}F_x$. Both $Li_xVO_{2-x}F_x$ and V[FeV]O_4 have open crystal structures with the ability to reversibly store lithium in interstitial lattice sites, and the effect of these compounds on capacity and cyclic stability of the LiF/Fe(V_2O_5) nanocomposites is discussed.

Keywords: Extended X-ray absorption fine structure (EXAFS, XANES); Nanocomposite; Li-ion battery; Mixed conductor; Iron fluoride

1. Introduction

The battery systems in use today are typically based on Li intercalation chemistry where the host lattice stays intact upon cycling and up to one Li per formula unit is transferred during the charge and discharge processes. This limits the total capacity of a typical transition metal oxide material to 140–220 mA h g^{-1} [1]. Further increase of the capacity can only be achieved by using a different operation principle, and novel materials, which are based on the conversion principle, are being extensively studied [2]. These conversion materials are able to transfer up to three electrons per transition metal, and as a result the energy densities are multiplied by the number of transferred electrons. Typical theoretical specific capacities of metal fluorides with high operating voltages (>2 V) suitable for cathodes are in the order of 500–750 mA h g^{-1} [3], up to five times higher than the earliest commercially available $LiCoO_2$ intercalation compound. In $LiCoO_2$, the theoretical capacity of the cell is relatively low, at ~130 mA h g^{-1},

* Corresponding author. Tel.: +49 721 608 26377; fax: +49 721 608 28298.
E-mail address: alexander.pohl@kit.edu (A.H. Pohl).

http://dx.doi.org/10.1016/j.actamat.2014.01.016
1359-6454/

because only 0.5 Li/Co can be reversibly cycled without causing cell capacity loss due to changes in the $LiCoO_2$ structure [1].

Fluorides have the advantage over other conversion materials such as nitrides, oxides and sulfides [2], in that the operation voltage is high due to the strong fluoride bond. The F^- ion has the highest electronegativity in the periodic table and forms highly ionic M–F bonds. Consequently, metal fluorides have an intrinsically high band gap and are insulators, making it difficult to apply them directly as cathode materials.

The traditional approach to enable reversible cycling of transition metal (TM) fluoride cathodes is to mix the insulating fluoride with conductive carbon [4,5]. The MF_x/carbon composite materials show a good initial discharge capacity, but cyclic stability is poor unless a high fraction of carbon is added. The next attempt to improve the cycle life of TM fluorides was to embed the material into a matrix of mixed ionic and electric conductors. The mixed conducting matrix (MCM) is typically a metal or semimetal with the ability to intercalate Li at potentials higher than the TM conversion potential due to its open crystal structure. A number of TM fluorides have been enabled with MCMs:

(a) Badway et al. [6] showed a near theoretical discharge capacity of a $CuF_2(MoO_3)$ composite, although reversible cycling was not possible. The mechanism of the CuF_2 transformation into nanoscale Cu particles was established in a later paper using in situ X-ray absorption spectroscopy (XAS) [7] and it was proven by comparison with macro-sized CuF_2 that the improvement in discharge capacity was directly related to the MoO_3 additive.
(b) Gmitter et al. [8] investigated the catalytic behaviour of extremely small Bi metal particles on the decomposition of cyclic and acyclic carbonate electrolytes in a $BiF_3(MoS_2)$ composite.
(c) Wu et al. [9,10] investigated the $FeF_3(V_2O_5, MoS_2)$ systems in two short papers. They started with the charged state FeF_3 and showed for the V_2O_5 doped material a near-theoretical capacity of 209 mA h g^{-1} for the $1e^-$ transfer in the voltage range 4.5–2.0 V. The conversion reaction of FeF_2 into Fe in the voltage range 2.0–1.3 V was not investigated and no mechanistic details about the mode of action of the MCM additive were given in the papers.

Adding V_2O_5 to the discharged state LiF/Fe has the advantage that the as-prepared cathode contains a source of lithium and could in principle be directly combined with a carbonaceous anode, but this has not been studied to date. We recently prepared LiF/Fe(V_2O_5) nanocomposites with varying V_2O_5 content of 0, 10, 15 and 20 wt.% by high-energy ball milling and found a superior improvement in cyclic stability and capacity utilization compared to the non-doped control composite (Fig. 1a) [11]. For the

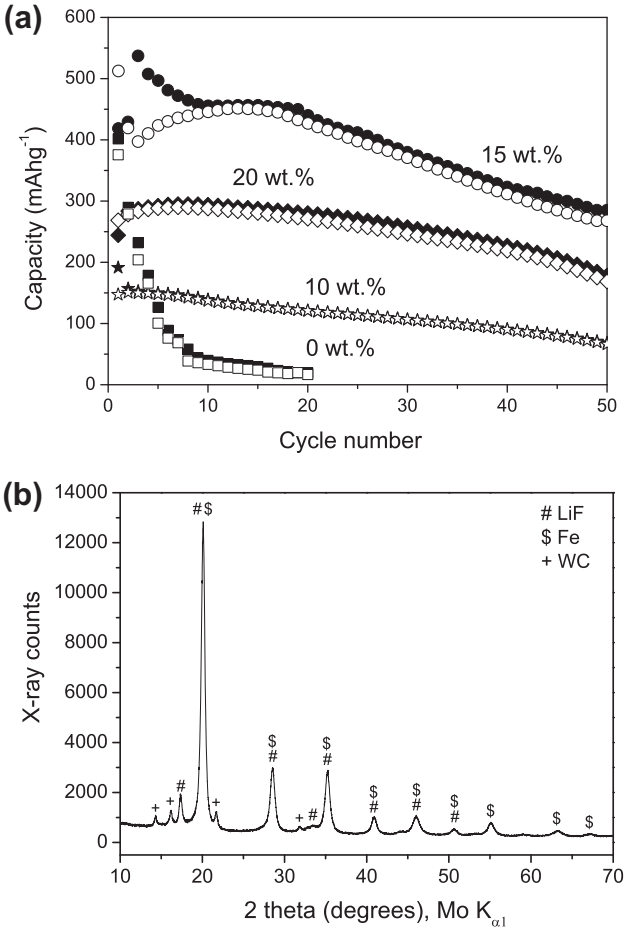

Fig. 1. (a) Cycle performance of Fe/LiF(V_2O_5) nanocomposites with 10, 15 and 20 wt.% V_2O_5 and the control composite without addition of V_2O_5 (open symbols charge, closed symbols discharge, 20 mA g^{-1}, 1.3–4.3 V, 30 h ball mill time). (b) XRD pattern of the as-prepared 15 wt.% LiF/Fe(V_2O_5) nanocomposite. Symbols denote identified phases ($\lambda = 0.7093$ Å).

15 wt.% LiF/Fe(V_2O_5) composite, we obtained a specific capacity of 420 ± 5 mA h g^{-1} (total weight) for a period of 20 cycles without a noticeable reduction in capacity, and afterwards $\sim 270 \pm 5$ mA h g^{-1} up to the 50th cycle. Surprisingly, the X-ray diffraction (XRD) pattern of the as-prepared 15 wt.% LiF/Fe(V_2O_5) composite (Fig. 1b) shows no reflections from V_2O_5 or any new phases, but only reflections from the LiF and Fe starting materials. As the vanadium-containing phases in the as-prepared composite and during cycling could not be determined from XRD, we collected in situ XAS data at the *Institut für Nukleare Entsorgung* (INE) beamline of the ANKA synchrotron during the first charge (Fe K-edge) and first discharge (V K-edge) of the battery cell. We were interested in determining the oxidation state and local structure of the vanadium- and iron-containing species in these composites.

This paper is divided into two parts. In the first part, the Fe and V valence states during cycling are extracted from the chemical shift of the in situ X-ray absorption near edge structure (XANES) spectra and the Fe local structure

determined from extended X-ray absorption fine structure (EXAFS) analysis. In the second part, we identify the new mixed conducting matrices formed during ball milling of LiF, Fe and V_2O_5 using a combination of principal component analysis (PCA), Mössbauer spectroscopy and theoretical calculations of XANES spectra of model compounds. We then discuss the mechanistic details of how the newly formed lithium and iron vanadates are able to improve capacity and cyclic stability of the LiF/Fe(V_2O_5) composites.

2. Experimental

2.1. Sample preparation

V_2O_5 (Sigma–Aldrich, 99.6%), Fe metal powder (Alfa Aesar, ~20 mesh, 99%) and LiF (Alfa Aesar, 99.99%, Puratronic) were stored in an argon-filled glove box and used as-received without further purification. Nanocomposites with (a) 15 wt.% V_2O_5 and a fixed Fe:LiF ratio of 1:3, (b) Fe:V_2O_5 (1:2) and (c) LiF:V_2O_5 (1:1) were prepared by high-energy ball milling using a Fritsch planetary ball mill. The starting materials were loaded into a 250 ml milling vial made of WC and sealed inside the glove box. Ball-milling of the powder mixtures was conducted at 400 rpm for 20 h with a ball-to-powder ratio of 60.

2.2. Characterization methods

2.2.1. Electrochemical characterization

Electrodes for in situ characterization were prepared by adding 15 wt.% poly(vinylidene fluoride-co-hexafluoropropylene) (Kynar 2801, Elf Atochem), 15 wt.% carbon black (Super C65, Timcal) and a few drops of *N*-methyl-2-pyrrolidone (Sigma Aldrich, 99.5%) to 70 wt.% LiF/Fe(V_2O_5) composite. The slurry was cast onto glassy carbon films (60 μm, HTW Germany) and a home-built battery cell was assembled in an argon-filled glove box using two PE/PP/PE sheets (Celgard) as separator and saturated with electrolyte (LP30, Merck) consisting of 1 M $LiPF_6$ dissolved in a 1:1 mixture of ethylene carbonate and dimethyl carbonate. The cells were tested in galvanostatic mode at the beamline at 25 °C vs. Li foil (Goodfellow, 0.2 mm, 99.9%) at a constant current of 0.1 mA.

2.2.2. Physical characterization

Powder XRD patterns of the ball-milled nanocomposites were collected using a STOE Stadi P diffractometer equipped with a Dectris Mythen 1K linear silicon strip detector and Ge(1 1 1) double crystal monochromator (Mo $K\alpha_1$ radiation, $\lambda = 0.7093$ Å) in Debye–Scherrer capillary mode. The samples were loaded into 0.7 mm glass capillaries (Hilgenberg borosilicate glass No. 50) in an argon-filled glove box. Profiles were refined using the TOPAS software package [12].

For XAS measurements of reference materials, ~10 mg FeF_3, FeF_2, V_2O_5 and V_2O_3 were diluted with ~60 mg spectroscopic grade polyethylene and pressed into 12 × 1 mm discs using a Spex X-Press 3635 pellet press with a pressure of 10 T within 2 min. The sample discs were taped on a U-shaped sample holder with Kapton tape and placed into the X-ray beam for transmission measurements. For in situ measurements, the battery cell was placed vertically into the X-ray beam and XAS data of the LiF/Fe(V_2O_5) nanocomposite were collected in transmission mode.

The synchrotron light source from a 1.5 T bending magnet at the INE beam line was monochromated using a Lemonnier-type Si(1 1 1) double crystal for the Fe K-edge (7.112 keV) and the V K-edge (5.465 keV), and was detuned by 70% for harmonic rejection. The absorption was measured using three ionization chambers filled with N_2 gas and equipped with Femto low current amplifiers. The pre-edge region, −200 to −30 eV, was scanned with 3 eV s^{-1} up to −50 eV and afterwards with 2 eV s^{-1}, and the edge region, −30 to 30 eV, was scanned with 0.5 eV s^{-1} (relative to the absorption edge energy). The post-edge region, $k =$ 2.8–16.0 $Å^{-1}$, was scanned with 0.03 $Å^{-1}$ s^{-1} with the accumulated time proportional to $k^{0.5}$. For in situ measurements, the energy ranges for the Fe K-edge and V K-edge were reduced to $k =$ 14 $Å^{-1}$ and 13 $Å^{-1}$, respectively, for a collection time of ~30 min per spectrum. For V K-edge spectra, the edge region, −20 to 30 eV, was scanned with a speed of 0.25 eV s^{-1}. Spectra were aligned, merged and the background subtracted with Athena [13].

Mössbauer spectra were recorded using a constant acceleration-type spectrometer in transmission geometry with a moving source of ^{57}Co in a Rh matrix. Approximately 50 mg LiF/Fe(V_2O_5) composite was sealed into a plastic bag inside an argon-filled glove box. The isomer shift is given relative to α-Fe at room temperature.

2.2.3. Theoretical calculations

EXAFS data were analysed using the multiple scattering approach implemented within Feff 6L [14] and V–O bond distances were determined from the Fourier transform (FT) of $k^2\chi(k)$ using Larch [15]. PCA was performed using Fitit [16].

Calculations of XANES spectra were performed for the set of possible compounds that could represent vanadium local structure in the ball-milled composite. We have used full-potential linearized augmented plane-wave approximation (FLAPW) implemented in the Wien2k program package [17,18]. The generalized gradient approximation within the Perdew, Burke, Ernzerhof exchange–correlation functional (GGA PBE) [19] was used for treatment of the exchange–correlation interactions. It was found that V K-edge XANES in the present compounds are well reproduced in the ground state approximation without a core hole. The plane wave basis set and the number of *k*-points in the reciprocal lattice were increased until variations in the calculated spectral shape were converged. Energy convergence in the self-consistent iteration procedure was better than 1 meV. The core-level energies and Fermi level

position were obtained from FLAPW simulations and were used to determine the relative energy shift of the calculated XANES spectra since this information was not available for all model compounds. The charge state of V was determined from Bader analysis [20,21] of the electron density for V reference compounds and model structures. The theoretical procedure is validated in Fig. S.1 for V_2O_3 and V_2O_5 reference compounds.

3. Results

3.1. Part I: Valence states and local structure from in situ XANES spectra

Voltage vs. time plots and the XANES spectra collected at selected points are shown in Fig. 2. On the first charge, the iron edge position shifts to higher energies, indicating oxidation of Fe and at the same time the intensity of the main edge increases. On the second discharge, there are two small plateaus in the region 3.2–2.0 V followed by a long plateau at 1.8 V. In the V K-edge XANES spectra, the vanadium pre-edge peak intensity decreased and the intensity of the main edge increased. The FTs of $k^2\chi(k)$ of selected in situ spectra collected at the Fe K-edge are shown in Fig. 3a. A peak at 1.5 Å, which corresponds to Fe–F distances in rutile FeF_2, starts to emerge as the voltage of the battery is raised from 2.0 to 4.2 V. At the same time, the intensities of the first and third peaks at 2.20 Å and 4.50 Å, respectively, which correspond to Fe–Fe distances in metallic Fe, are reduced. In the V K-edge FT $k^2\chi(k)$ (Fig. 3b), there is only one coordination shell at 1.6 Å corresponding to the first V–O distances, which changes very little in intensity and position as the battery is discharged. Second or third coordination shells at higher r are completely absent, highlighting the amorphous nature of the phase formed during ball milling. We fitted the positions of the first peak in FT $k^2\chi(k)$ in the series of spectra (a typical fit is shown in Fig. S.2) and obtained a range of V–O bond distance of 2.02–2.08 Å (cf. Table S.1) during cycling. The average V–O distance of 2.04(2) lies well within the range of values (1.94–2.08 Å) found for V in octahedral coordination in various vanadium oxides, lithium vanadium oxides and iron vanadates (cf. Table S.2). The V–O bond distances did not change much during cycling, indicating that no major structural transformations occurred.

Kunzl's law states that the energy shift varies linearly with the valence of the absorbing atom [22]. The spectra of V metal, V_2O_3 and V_2O_5 have well defined pre-edge peaks and from the position of the pre-edge an oxidation state calibration curve was constructed (cf. Fig. S.3). The change of the pre-edge position in the V K-edge spectra of the cell was used to determine the vanadium oxidation state during the first discharge of the cell. Fig. 4 shows that the V oxidation state changed from $V^{3.9+}$ at 4 V to $V^{3.5+}$ at 1.7 V after 22 h of discharge. If we assume that $Li_xV_2O_5$ has formed, this oxidation state range would correspond to $x = 2.2$–2.9, consistent with the maximum Li intercalated compound $Li_3V_2O_5$ [23]. In the case of Li_xVO_2, x would correspond to 0.10–0.45, consistent with deintercalation of $LiVO_2$, where Li can be extracted up to $x = 0.1$ [24].

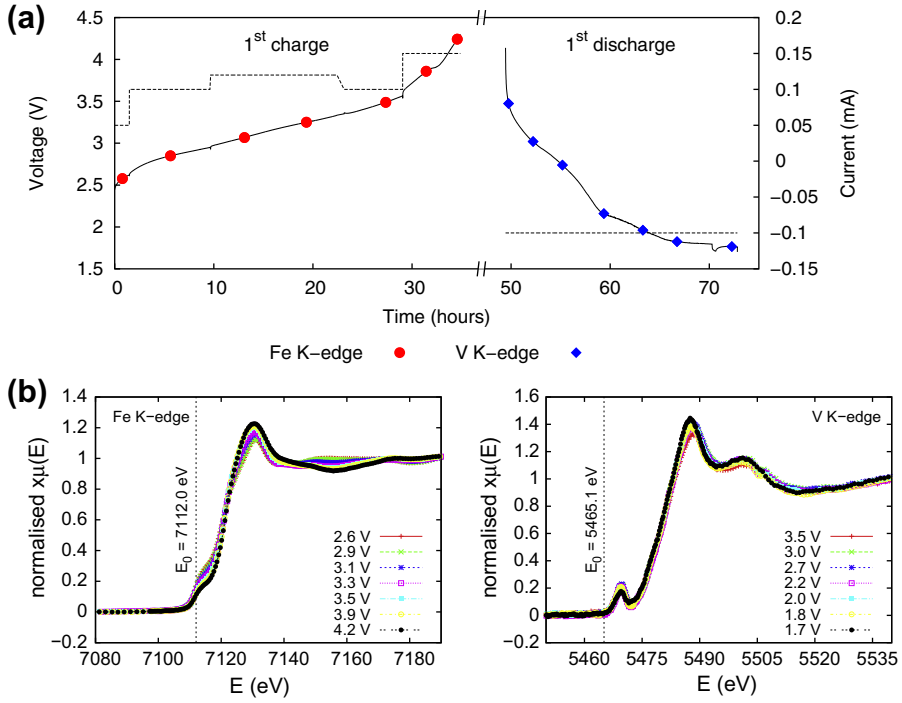

Fig. 2. (a) Voltage and current vs. time plots of the in situ battery cell of the LiF/Fe(V_2O_5) composite (top) showing first charge from 2.6 to 4.2 V and first discharge from 3.5 to 1.7 V (solid line voltage, dashed line current). The symbols (●, ♦) indicate where in situ XAS spectra have been collected at Fe K-edge (bottom left) and V K-edge (bottom right).

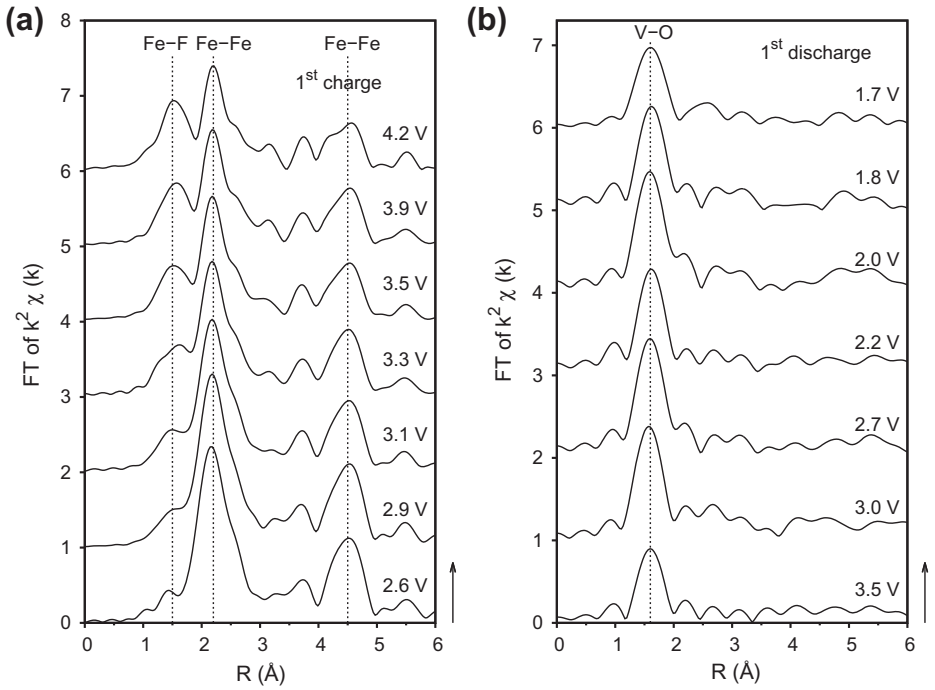

Fig. 3. FTs of $k^2\chi(k)$ collected (a) during first charge at the Fe K-edge and (b) during first discharge at the V K-edge of the in situ battery cell. The plots are offset by 1 and the *R*-scale was not corrected for the phase shift of the absorber atom.

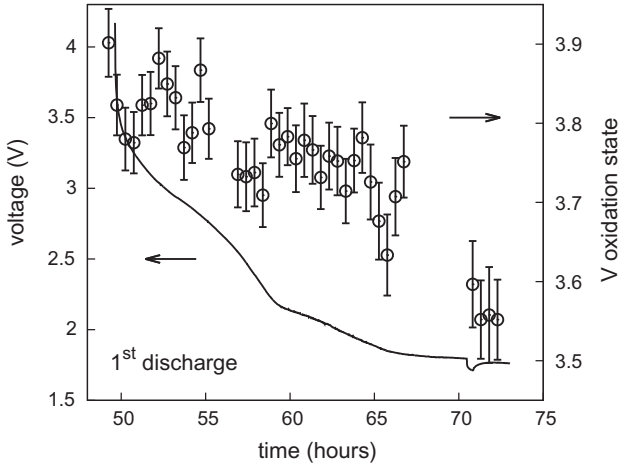

Fig. 4. Evolution of the vanadium valence state obtained from V K-edge XANES spectra during first discharge of the battery cell.

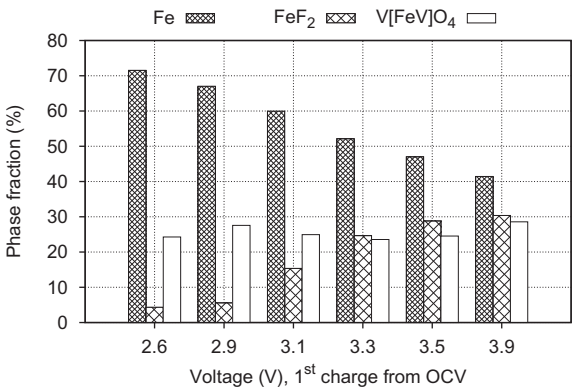

Fig. 5. PCA of the series of Fe K-edge spectra collected during first charge showing the concentrations of the components Fe, FeF_2 and the spinel $V[FeV]O_4$.

We conclude that from a point of the V oxidation state, the formation of both $Li_xV_2O_5$ and Li_xVO_2 phases during the first discharge could be possible. Further analysis of the vanadium local atomic structure along with verification of Fe K-edge EXAFS data is based on quantitative theoretical analysis of XANES data.

3.2. Part II: Identification of the mixed conducting matrix

3.2.1. PCA

We have used the PCA [16] tool to mathematically decompose the series of the Fe K-edge spectra at different voltages into independent sub-spectra. It was found that the series of spectra can be reproduced as a combination of three components. To obtain the concentrations of these components and the corresponding XANES spectra, we have assumed that the main component in the composite is pure iron (this is confirmed also by Mössbauer data). The shapes of the other two components were determined using physical constraints – the concentrations should be positive and concentration of the component responsible for lithium storage should be constant (cf. Fig. S.4). The PCA analysis shown in Fig. 5 confirms that Fe/LiF converts into FeF_2 during charge, and at 3.9 V the concentration of FeF_2 has reached ~35 wt.%. Surprisingly, we found that ~25 wt.% of a new component was already present in the as-prepared cell at open circuit potential,

although no current was applied to the cell yet. Therefore, the new phase could not have formed electrochemically, but must have formed during ball milling. Since there are no new phases in the XRD pattern (cf. Fig. 1b) of the as-prepared 15 wt.% LiF/Fe(V_2O_5) composite, this phase should be amorphous. As will be shown below, the third component can be regarded as a highly disordered inverse spinel V[FeV]O_4 with short range order of octahedral and tetrahedral coordination polyhedra. To confirm our initial guess, we used Mössbauer spectroscopy to determine the Fe valence state in the as-prepared composite and theoretical calculations of XANES spectra for V compounds with tetrahedral and octahedral V coordination.

3.2.2. Mössbauer spectroscopy

The Mössbauer spectrum of the as-prepared 15 wt.% LiF/Fe(V_2O_5) composite shows a large sextet from metallic Fe^0, a smaller Fe^{2+} doublet and a very small Fe^{3+} singlet (Fig. 6a). The corresponding Mössbauer parameters are summarized in Table 1. The presence of a Fe^0 sextet rather than a doublet or singlet indicates that the Fe grains after ball milling must be larger than ~6 nm, the critical grain size where the Fe hyperfine splitting disappears due to the very small size of the Fe particles [25]. The Fe^{2+} doublet has an isomer shift (IS) of 1.02 mm s^{-1} and a large quadrupole splitting (QS) of 1.79 mm s^{-1}, which are both too small for crystalline or nanosize FeF_2 [26] (IS 1.33 mm s^{-1}, QS 2.78 mm s^{-1}). This precludes a simple reaction of Li with V_2O_5 with concomitant formation of FeF_2. Dyar et al. [27] have published a diagram which shows isomer shift vs. quadrupole splitting for a large number of rock-forming minerals. They identified clusters of parameters where iron in its most stable oxidation states Fe^0, Fe^{2+} and Fe^{3+} are either four-, six- or eight-fold coordinated. According to this study, an IS of 1.02 mm s^{-1} is indicative of a Fe^{2+} state in an octahedral environment and is compatible with an iron oxide spinel structure, and for Fe[V_2]-O_4, IS values of 1.13 mm s^{-1} [28], 1.07 mm s^{-1} [29] and 0.91 mm s^{-1} [30] have been reported.

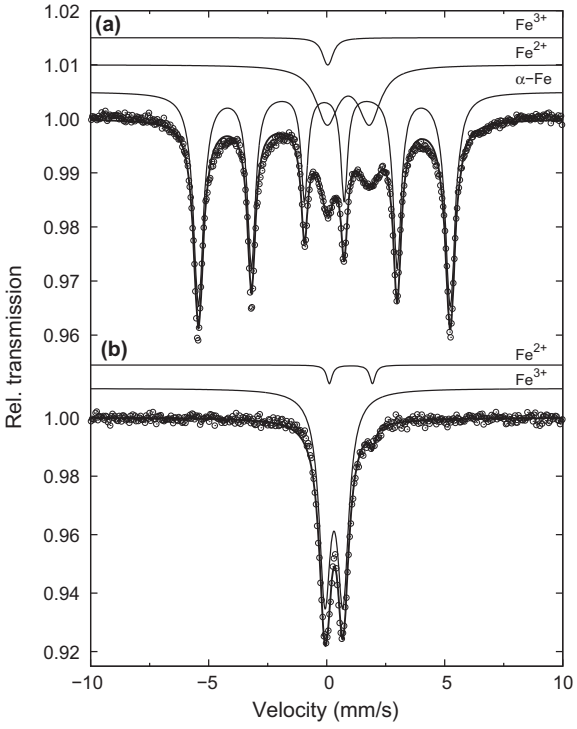

Fig. 6. Mössbauer spectra of the as-prepared LiF/Fe(V_2O_5) composite (top) and Fe(V_2O_5) (bottom). The isomer shift is given relative to α-Fe.

The Mössbauer spectra of the iron oxide spinels have been investigated by Gupta and Mathur [28] and Yagnik and Mathur [31] and show singlet or doublet resonance lines depending on which crystallographic site in A[B_2]X_4 spinel (A, B or both) the Fe ions are located. Fe ions located only on the tetrahedral A sites, denoted as Fe[M_2]-O_4, show a spectrum with a single line due to the a small electric-field gradient and hence a vanishing QS. Fe ions present only at octahedral B sites, denoted as M[Fe_2]O_4, show a spectrum consisting of one doublet with a quadrupole splitting due to the trigonal field (non-cubic symmetry) at the B sites. If additionally the metal ions (same element or different elements) on the B site have a different charge, the quadrupole splitting is enlarged due to the electric field gradient produced by the asymmetric charge distribution on the 12 neighbours of each A site. As we observe one doublet with a large QS of 1.79 mm s^{-1}, we conclude that the Fe^{2+} phase seen in both the XANES and Mössbauer spectra of the LiF/Fe(V_2O_5) composite could be the inverse spinel $V^{3+}[Fe^{2+}V^{3+}]O_4$, with Fe and V sharing the octahedral B sites. The Fe^{3+} singlet was included in the fit to account for the strong asymmetry of the Fe^{2+} doublet, which could be due to a very small amount of Fe^{3+} ions occupying the tetrahedral A site.

3.2.3. Comparison of XANES spectra with literature

At the simplest level, XANES spectra were compared with literature spectra and used as a fingerprint method. Fig. 7a shows the experimental V K-edge XANES

Table 1
Mössbauer parameters IS, quadrupole splitting QS and hyperfine splitting (BHF).

Composite	Oxide	Type	Area (%)	IS (mm s^{-1})	QS (mm s^{-1})	BHF (T)	Composition (wt.%)
LiF/Fe(V_2O_5)	α-Fe	Sextet	75.9	0.06	–	33.1	V_2O_5: 15.0
	Fe^{2+}	Doublet	21.6	1.02	1.79	–	LiF: 49.4
	Fe^{3+}	Singlet	2.5	0.25	–	–	Fe: 35.6
Fe(V_2O_5)	Fe^{2+}	Doublet	4.4	1.14	1.82	–	V_2O_5: 86.6
	Fe^{3+}	Doublet	95.6	0.41	0.77	–	Fe: 13.3

spectrum of the cell at open circuit voltage in comparison with vanadium oxide reference spectra measured by us and Wong et al. [32]. It can be seen immediately that none of the oxide spectra is matching the experimental spectrum of the LiF/Fe(V_2O_5) composite particularly well. The main edge of our experimental spectrum is much larger and the pre-edge much smaller compared to the starting material V_2O_5, indicating that a new compound was formed. Spectra with distorted octahedral VO_6 coordination, i.e. VO_2, V_4O_7 and V_2O_3 (cf. Fig. 7a and Table S.2), seems to have the right intensity of the pre-edge, but our experimental spectrum shows a much higher intensity of the main absorption edge.

A good match for our experimental spectrum is found with $Li_xV_2O_5$ prepared by chemical Li intercalation into the V_2O_5 host lattice (Fig. 7b) [33]. With increasing lithium concentration x, the main edge intensity increases and the pre-edge decreases. The best match is found at a maximum intercalation of $x = 2.46$. Unfortunately, the structure of $Li_xV_2O_5$ ($x > 1$) is not known and highly disordered, and Li-intercalation was found to be irreversible when $x > 1$ [34]. The mixed conducting matrix, however, can only be effective if Li intercalation, and therefore Li ionic conductivity, is reversible. As experimental XANES data on lithium and iron vanadates are sparse, in the following section we perform calculations for different in the literature available Li–V–O phases and Fe–V–O phases with tetrahedral and octahedral V coordination and compare them with the experimental XANES spectrum of the ball-milled composite.

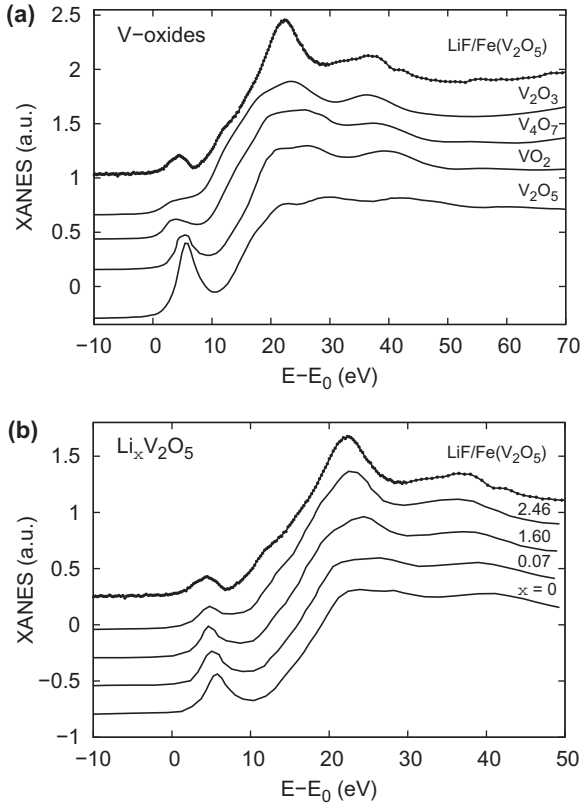

Fig. 7. Comparison of the XANES spectrum of the as-prepared LiF/Fe(V_2O_5) nanocomposite (black dots) with spectra of (a) vanadium oxides (data for VO_2 and V_4O_7 taken from Ref. [32]) and (b) chemically lithiated $Li_xV_2O_5$ (data taken from Ref. [33]). The energy is plotted relative to the V K-edge energy of 5.465 keV.

3.2.4. Theoretical calculation of XANES model spectra

Fig. 8 shows the simulations for several Li–V–O and Fe–V–O compounds with known crystal structures. XANES probes a short range order and the photoelectron wave scatters efficiently only within 1 nm around the photo-excited atom. In the case of our nanocomposite, the contribution to the X-ray absorption signal from amorphous phases and from nanocrystallites with a size of 1 nm would be similar. Both these cases cannot be detected by laboratory XRD.

Considering the high main edge intensity of the experimental spectrum, octahedral VO_6 coordination as found e.g. in $LiVO_2$ is more probable than square-pyramidal VO_5 or tetrahedral VO_4 coordination. The spectra of LiV_2O_5 with square-pyramidal or $FeVO_4$ and $LiVO_3$ with tetrahedral V coordination show intense pre-edge features due to *p–d* hybridization effects [35]. However, the oxygen octahedra around vanadium in $LiVO_2$ are not distorted, and

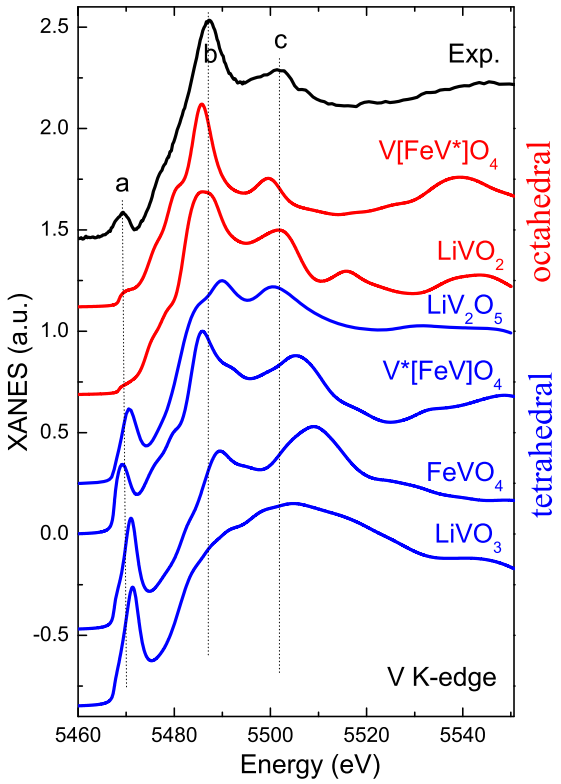

Fig. 8. FLAPW calculations for the series of lithium vanadates and iron vanadates with local octahedral (red) and tetrahedral (blue) vanadium environment. Upper black curve is the experimental V K-edge XANES spectrum for the ball-milled composite with (a) pre-edge, (b) main edge and (c) post-edge peaks. V[FeV]O_4 has vanadium on two non-equivalent sites denoted by ($\bullet^*$) and both sub-spectra are shown. (For interpretation of the references to color in this figure legend, the reader is referred to the web version of this article.)

thus the pre-edge intensity is smaller than in the experiment. The inverse spinel V[FeV]O_4, which we derived from $Fe^{3+}[Fe^{2+}V]O_4$ by changing the Fe^{3+} atom on the tetrahedral site (8*a*) into a V^{3+} atom [36], is a special case as the crystal structure consists of both V in octahedral as well as in tetrahedral coordination. We calculated V K-edge XANES spectra for the two non-equivalent V positions in V[FeV]O_4. The superimposed spectrum shown in Fig. 9a has therefore a pre-edge due to *p–d* hybridization in tetrahedral coordination and a high main edge due to V in octahedral coordination, and resembles the experimental spectrum well. Additionally, the calculated Fe K-edge spectrum of V[FeV]O_4 shown in Fig. 9b also matches the PCA spectrum of the new Fe^{2+} component and shows a very high main edge due to Fe on the octahedral sites.

3.2.5. Reactions of Fe and LiF with V_2O_5

As the new lithium and iron vanadates in LiF/Fe(V_2O_5) are amorphous, we tried to prepare more crystalline compounds in higher concentrations by ball milling mixtures of LiF(V_2O_5) and Fe(V_2O_5) and to see whether LiF and Fe could be independently inserted into the structure of V_2O_5.

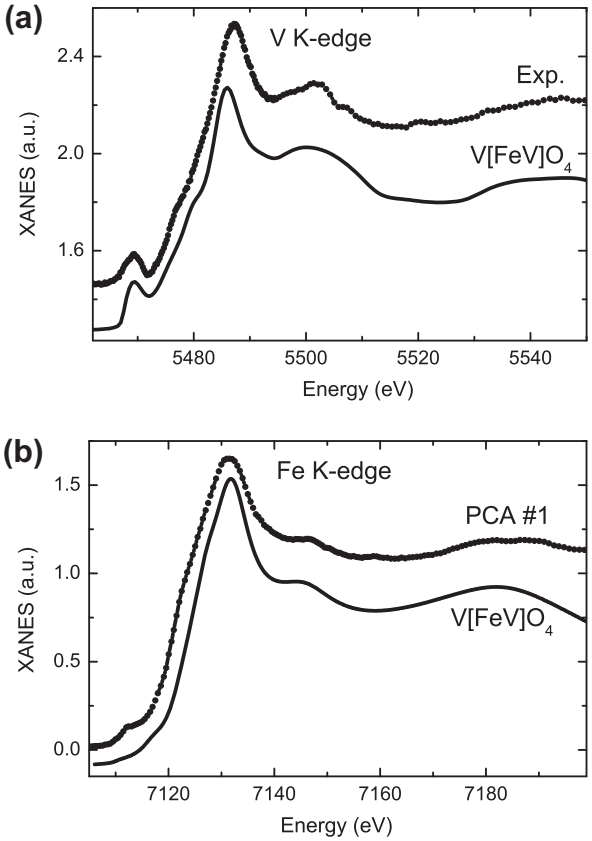

Fig. 9. Comparison of the FLAPW theoretical spectra of the mixed conducting matrix V[FeV]O_4 with (a) the experimental V K-edge spectrum of LiF/Fe(V_2O_5) and (b) the extracted Fe K-edge PCA spectrum of the new phase. The total V K-edge spectrum of V[FeV]O_4 was obtained by a superposition of spectra with octahedral and tetrahedral V positions (cf. Fig. 8).

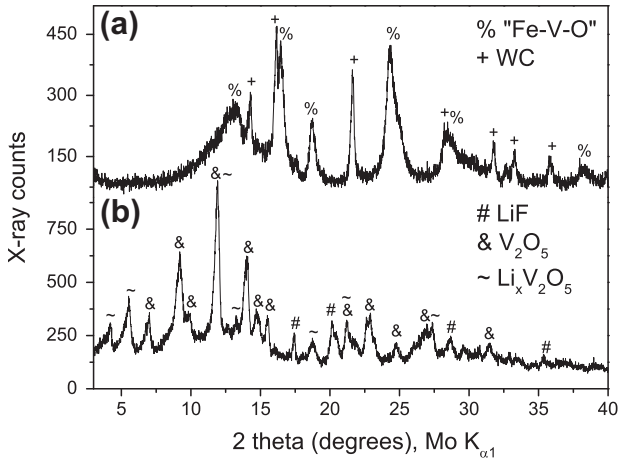

Fig. 10. XRD patterns of as-prepared nanocomposites: (a) Fe(V_2O_5) and (b) LiF(V_2O_5). Symbols denote identified phases ($\lambda = 0.7093$ Å).

After ball milling Fe(V_2O_5), we observed a colour change from orange/grey to black, with a similar black colour as the LiF/Fe(V_2O_5) composite used for the XAS experiments. The XRD pattern in Fig. 10a shows reflections of a new, highly disordered phase. The Mössbauer spectrum of the Fe(V_2O_5) composite in Fig. 6b consists of a large Fe^{3+} doublet and a small Fe^{2+} doublet (cf. Table 1). Both doublets are compatible with Fe on octahedral B sites in iron oxide spinels [27], but it is not clear from XRD that the compound formed is single phase. The XRD pattern of LiF(V_2O_5) in Fig. 10b shows reflections of the starting materials V_2O_5 and LiF, and reflections of a new phase, which could be indexed on a monoclinic cell with $a = 10.102(4)$ Å, $b = 3.602(1)$ Å, $c = 15.347(6)$ Å and $b = 109.79(4)°$ ($A2/m$, $R_{wp} = 10.13\%$) and identified as $Li_xV_2O_5$ [37].

4. Discussion

From calculations of both Fe and V K-edge XANES spectra of model structures with tetrahedral and octahedral V coordination, the V[FeV]O_4 inverse spinel and $LiVO_2$ are good candidates for the MCMs formed during preparation. The fraction of the octahedrally coordinated vanadium in the $LiVO_2$ cannot be excluded because of the similarity of the V K-edge XANES spectra for the series of octahedrally coordinated compounds. During cycling, Fe converts into FeF_2 and the concentration and structure of the mixed conducting matrices V[FeV]O_4 and $LiVO_2$ change very little during charge/discharge since changes in V K-edge XANES are very small. The formation of V[FeV]O_4 according to

$$V_2O_5 + Fe \rightarrow V[FeV]O_4 + 1/2\ O_2 \quad (1)$$

is supported by the Mössbauer spectrum, which indicates that Fe was oxidized to Fe^{2+} and the Mössbauer parameters are compatible with Fe on the octahedral site in the spinel structure. From the Fe(V_2O_5) and LiF(V_2O_5) composites, it is known that it is possible to intercalate both Li or LiF

with concomitant F^-/oxygen exchange and Fe into the structure of V_2O_5 under ball milling conditions. As soon as metallic Fe is in the reaction mixture, the composite turned black, indicating that a reaction took place. But when using LiF without Fe, we did not observe a colour change and the V_2O_5 framework stayed intact. Most probably the presence of Fe leads to the formation of a cubic spinel framework with a rearrangement of VO_5 layers. Fe in its compounds is usually in the form of Fe^{2+} and Fe^{3+} valence states and is therefore able to donate electrons for the reduction of V^{5+}. Consequently, ball milling FeF_3 with V_2O_5 does not form new phases as Fe is already in its highest Fe^{3+} oxidation state [9]. V_2O_5 consists of layers made from edge and corner sharing VO_5 square pyramids with alternating pairs of pyramids pointing upwards and downwards [38]. There is plenty of space between the layers to accommodate other metal ions such as Li^+, e.g. ε-LiV_2O_5 [39] and Ca^{2+}, e.g. CaV_2O_5 [40]. The reducing strengths of Fe metal under ball milling conditions leads to a reduction of V^{5+} and a concomitant rearrangement of the VO^5 layers into a three-dimensional (3-D) $[V_2]O_4$ spinel framework. In the V[FeV]O_4 spinel, the O^{2-} anions form a cubic-close-packed array, and the V cations on the A site occupy 1/8 of the 8*c* tetrahedral interstices and Fe/V on the B site occupy 1/2 of the 16*d* octahedral sites. Consequently, Li insertion into spinels occurs via diffusion through 3-D channels of vacant tetrahedral and octahedral interstices.

Little is known about the Li intercalation chemistry of iron vanadates, especially the electrochemical potential at which this process occurs. In the vanadium oxide spinel $Li_xV_2O_4$, Li can be inserted topotactically at a potential of 2.2 V with retention of the $[V_2]O_4$ framework up to a composition of $Li_2V_2O_4$ [41]. During lithiation, Li fills the 16*c* octahedral vacancies and Li on the tetrahedral 8*a* sites is displaced to the 16*c* sites giving a defect rock-salt structure. In theory, it should be possible to lithiate V[FeV]O_4, but this has not been studied yet. The isostructural V[ZnV]O_4 spinel [42] has a peak in the cyclovoltammogram in the range 1.8–2.2 V, compatible with the plateau at 2.0–2.2 V in the first discharge curve of our composite. It would be possible that this plateau corresponds to Li insertion into V[FeV]O_4, assuming that the potentials of Zn and Fe are similar. In general, the voltage of the oxide spinels can be tailored by changing the metal cation on the B sites of the framework [43].

The formation of $LiVO_2$ occurs most likely via intercalation of LiF into V_2O_5 according to

$$V_2O_5 + xLiF \rightarrow Li_xVO_{2-x}F_x + 1/2\ O_2 \quad (2)$$

and the VO_5 pentagonal pyramids rearrange into layers of edge-sharing VO_6 octahedra as found in ε-$LiVO_2$ [39]. The space between the layers in $Li_xVO_{2-x}F_x$ is occupied by Li^+ cations and the F^- anions are incorporated into the structure as $VO_{6-x}F_x$ mixed octahedra. Such F^-/O^{2-} anion exchange has been previously observed in $CuF_2(MoO_3)$, where during ball milling $MoO_{3-x}F_x$ was formed [6,7]. $LiVO_2$ is a good electronic conductor with better performance compared to the well-known V_2O_5. The high electronic conductivity is arising from the mixed valence V^{3+}/V^{5+} and from structural resistance to lattice shearing during cycling. VO_2 aerogels show capacities as high as 500 mA h g^{-1} [44] and intercalate Li at a potential of 2.5 V, compatible with the first plateau at 3.2–2.5 V in the discharge curve of our composite. The V oxidation state of the LiF/Fe(V_2O_5) composite changed from $V^{3.9+}$ to $V^{3.5+}$ during the first discharge, which is very likely due to Li intercalation into $Li_xVO_{2-x}F$ and V[FeV]O_4. During high-energy ball milling, solid state reactions such as metathesis reactions, anion exchange and structural rearrangements are promoted because of the very high local heat and mechanical force induced into the reaction mixture by the planetary milling process.

5. Conclusions

We found that the addition of V_2O_5 to a mixture of Fe and LiF improves the cycle life of the composite dramatically. A stable capacity of 400 mA h g^{-1} was obtained over 25 cycles, enabling the reversible cycling of the material. During ball milling of LiF/Fe(V_2O_5), an MCM consisting of $Li_xVO_{2-x}F_x$ and V[FeV]O_4 phases is formed, which is responsible for the performance improvement. The Fe/LiF nanodomains are able to convert to FeF_2 only if electrons and Li ions can be delivered to the Fe/LiF particles simultaneously. This works because the MCM has an open structure and can conduct Li ions, and at the same time electrons because of its semi-metallic properties. The MCM is therefore able to achieve what, for example, conductive carbon alone could not do. We found that the V oxidation state was reduced from V^{5+} to $V^{3.9+}$ during ball milling and further to $V^{3.5+}$ during the first discharge. The XANES spectrum of the LiF/Fe(V_2O_5) composite could be reproduced with a number of model compounds with tetrahedral and octahedral V coordination. Among the calculated structures, $LiVO_2$ and V[FeV]O_4 show the best agreement with the experimental spectrum. $LiVO_2$ has regular VO_6 octahedra which are responsible for a main edge with high intensity, whereas V[FeV]O_4 has V on tetrahedral and octahedral lattice sites and produces a high main edge and a pre-edge peak due to VO_4 coordination. The combination of these two compounds reproduces the experimental spectrum remarkably well.

Acknowledgements

The authors gratefully acknowledge the ANKA synchrotron light source of the Karlsruhe Institute of Technology for granting beam time on the INE beam line for the experiment. A.G., V.S. and A.S. would like to thank the Southern Federal University and the Russian ministry of education and science for financial support (Project No. 14.A18.21.1153).

Appendix A. Supplementary material

Supplementary data associated with this article can be found, in the online version, at http://dx.doi.org/10.1016/j.actamat.2014.01.016.

References

[1] Whittingham MS. Chem Rev 2004;104:4271.
[2] Cabana J, Monconduit L, Larcher D, Palacín MR. Adv Mater 2010;22:E170.
[3] Amatucci GG, Pereira N. J Fluorine Chem 2007;128:243.
[4] Badway F, Cosandey F, Pereira N, Amatucci GG. J Electrochem Soc 2003;150:A1318.
[5] Wang F, Yu H-C, Chen M-H, Wu L, Pereira N, Thornton K, et al. Nat Commun 2012;3:1201.
[6] Badway F, Mansour AN, Pereira N, Al-Sharab JF, Cosandey F, Plitz I, et al. Chem Mater 2007;19:4129.
[7] Mansour AN, Badway F, Yoon W-S, Chung KY, Amatucci GG. J Solid State Chem 2010;183:3029.
[8] Gmitter AJ, Badway F, Rangan S, Bartynski R, Halajko A, Pereira N, et al. J Mater Chem 2010;20:4149.
[9] Wu W, Wang Y, Wang X, Chen Q, Wang X, Yang S, et al. J Alloys Compd 2009;486:93.
[10] Wu W, Wang X, Wang X, Yang S, Liu X, Chen Q. Mater Lett 2009;63:1788.
[11] Das B, Pohl AH, Chakravadhanula K, Kübel C, Fichtner M. J Power Sources; submitted for publication.
[12] Coelho AA. TOPAS Academic V4.1. Coelho Software, Brisbane; 2007.
[13] Ravel B, Newville M. J Synchrotron Radiat 2005;12:537.
[14] Zabinsky S, Rehr JJ, Ankudinov A, Albers R, Eller M. Phys Rev B 1995;52:2995.
[15] http://xraypy.github.com/xraylarch/.
[16] Smolentsev G, Soldatov AV. Comput Mater Sci 2007;39:569.
[17] Blaha P, Schwarz K, Sorantin P, Trickey SB. Comput Phys Commun 1990;59:399.
[18] Blaha P, Schwarz K, Madsen GKH, Kvasnicka D, Luitz J. WIEN2k, Karlheinz Schwartz. Austria: Vienna University of Technology; 2013.
[19] Perdew JP, Burke K, Ernzerhof M. Phys Rev Lett 1996;77:3865.
[20] Bader RFW. International series of monographs on chemistry atoms in molecules. A quantum theory, vol. 22. Oxford: Clarendon Press; 1994.
[21] Bader RFW. Chem Rev 1991;91:893.
[22] Ahn CC. Transmission electron energy loss spectrometry in materials science and the EELS atlas. Weinheim: Wiley-VCH; 2004.
[23] Delmas C, Cognacauradou H, Cocciantelli J, Menetrier M, Doumerc J. Solid State Ionics 1994;69:257.
[24] Thackeray MM, de Picciotto LA, David WIF, Bruce PG, Goodenough JB. J Solid State Chem 1987;67:285.
[25] Liao P, MacDonald BL, Dunlap RA, Dahn JR. Chem Mater 2008;20:454.
[26] Ramasamy S, Jiang J, Gleiter H, Birringer R, Gonser U. Solid State Commun 1990;74:851.
[27] Dyar MD, Agresti DG, Schaefer MW, Grant C, Sklute EC. Annu Rev Earth Planet Sci 2006;34:83.
[28] Gupta MP, Mathur HB. J Phys C Solid State Phys 1975;8:370.
[29] Tanaka M, Tokoro T, Aiyama Y. J Phys Soc Jpn 1966;21:262.
[30] Rossiter MJ. J Phys Chem Solids 1965;26:775.
[31] Yagnik CM, Mathur HB. J Phys C Solid State Phys 1968;1:469.
[32] Wong J, Messmer RP, Maylotte DH. Phys Rev B 1984;30:5596.
[33] Giorgetti M. J Electrochem Soc 1999;146:2387.
[34] Pecquenard B, Gourier D, Baffier N. Solid State Ionics 1995;78:287.
[35] Yamamoto T. X-Ray Spectrom 2008;37:572.
[36] Bernier JC, Poix P. Ann Chim (Paris, Fr) 1967;2:81.
[37] Galy J, Darriet J, Casalot A, Goodenough JB. J Solid State Chem 1970;1:339.
[38] Šipr O, Šimůnek A, Bocharov S, Kirchner T, Dräger G. Phys Rev B 1999;60:14115.
[39] Satto C, Sciau P, Dooryhee E, Galy J, Millet P. J Solid State Chem 1999;146:103.
[40] Onoda M, Nishiguchi N. J Solid State Chem 1996;127:359.
[41] De Picciotto LA, Thackeray MM, Pistoia G. Solid State Ionics 1988;28–30:1364.
[42] Xiao L, Zhao Y, Yin J, Zhang L. Chemistry 2009;15:9442.
[43] Thackeray MM. J Electrochem Soc 1995;142:2558.
[44] Baudrin E, Sudant G, Larcher D, Dunn B, Tarascon J-M. Chem Mater 2006;18:4369.